Effects of Hydrogen Peroxide on Intergranular Stress Corrosion Cracking of Stainless Steel in High Temperature Water, (V)

Characterization of Oxide Film on Stainless Steel by Multilateral Surface Analyses

Yohei MURAYAMA[1], Tomonori SATOH[1], Shunsuke UCHIDA[1,*], Yoshiyuki SATOH[1], Shinji NAGATA[2], Toshio SATOH[3], Yoichi WADA[4] and Masahiko TACHIBANA[4]

[1]*Department of Quantum Science and Energy Engineering, Graduate School of Engineering, Tohoku University, 1 Aobayama, Aoba-ku, Sendai 980-8579*
[2]*Materials Design Division, Institute for Materials Research, Tohoku University, 2-1-1, Katahira, Aoba-ku, Sendai 980-8577*
[3]*Division of Materials Control, Institute of Multidisciplinary Research for Advanced Materials, Tohoku University, 2-1-1, Katahira, Aoba-ku, Sendai 980-8577*
[4]*Power and Industrial Systems R&D Laboratory, Hitachi, Ltd., 7-2-1, Ohmika-cho, Hitachi-shi, Ibaraki 319-1221*

The difference in electrochemical corrosion potential of stainless steel exposed to high temperature pure water containing hydrogen peroxide (H_2O_2) and oxygen (O_2) is caused by differences in chemical form of oxide films. In order to identify differences in oxide film structures on stainless steel after exposure to H_2O_2 and O_2 environments, characteristics of the oxide films have been examined by multilateral surface analyses, *e.g.*, X-ray diffraction (XRD), Rutherford back scattering spectroscopy (RBS), secondary ion mass spectroscopy (SIMS) and X-ray photoelectron spectroscopy (XPS). Preliminary characterization results of oxide films confirmed that the oxide film formed under the H_2O_2 environment consists mainly of hematite (α-Fe_2O_3), while that under the O_2 environment consists of magnetite (Fe_3O_4). Furthermore oxidation at the very surface of the film is much more enhanced under the H_2O_2 environment than that under the O_2 environment. It was speculated that metal hydroxide plays an important role in oxidation of stainless steel in the presence of H_2O_2. The difference in electric resistance of oxide film causes the difference in anodic polarization properties. It is recommended that several anodic polarization curves for specimens with differently oxidized films should be prepared to calculate ECP based on the Evans diagram.

KEYWORDS: BWR type reactors, hydrogen peroxide, oxide film, stainless steels, surface characterization, hematite, magnetite, electrochemical corrosion, intergranular corrosion, clacking

I. Introduction

Hydrogen water chemistry (HWC) has been applied to moderate corrosive circumstances in the primary cooling systems of boiling water reactors (BWRs).[1] The HWC effects are influenced not only by the amount of hydrogen injected into the feed water but also reactor types, *e.g.*, BWR-2 through -6, core size, shroud diameter, downcomer width, presence or absence of jet pumps and plant operational conditions, *e.g.*, power density and distribution, recirculation flow rate, dose rate and flow velocity at the downcomer region, and jet pump efficiency.[2,3] Oxygen and hydrogen peroxide concentrations change along the recirculation flow path so that corrosive circumstances differ between locations in the primary cooling systems.[3]

Several indexes for corrosive circumstances have been proposed to evaluate the effects of HWC in BWR plants.[4–7] One of the most common indexes of corrosive circumstances is electrochemical corrosion potential (ECP).[5–7] Electrochemical corrosion potential is determined by a combination of surface conditions of a specimen and concentrations of oxidants, *e.g.*, oxygen, hydrogen peroxide and other corrosive radiolytic species. Unfortunately, most data concerning the effects of ECP on intergranular stress corrosion cracking (IGSCC) have been obtained by changing oxygen concentra-

tion. There are only limited data concerning the relationship between hydrogen peroxide concentration, ECP, and generation and propagation of IGSCC.[8] One of the reasons why fewer experimental data dealing with hydrogen peroxide have been reported is the difficulty of making experimental measurements because of hydrogen peroxide decomposition at elevated temperatures.

Decomposition of hydrogen peroxide is divided into two processes: (1) bulk decomposition (thermal decomposition in the bulk water);[9,10] and (2) surface decomposition (decomposition by contact with metal surfaces).[9,10] In the case of the reactor water, the extent of surface decomposition is a hundred times more than that of bulk decomposition.[3] In order to establish conditions with less temperature fluctuation and less concentration depression at the point of interest, the authors have tried using a polytetrafluoroethylene (PTFE) liner to get less surface decomposition[9,10] and they fabricated an experimental apparatus consisting of an autoclave with the PTFE inner liner and connecting branch lines with PTFE inner liner for hydrogen peroxide injection at the autoclave inlet and sampling at the autoclave outlet.[11]

Measured electrochemical corrosion potential (ECP) of type 304 stainless steel obtained in a high temperature, high pressure water loop showed hydrogen peroxide (H_2O_2) resulted in a much higher ECP than oxygen (O_2) with the same oxidant concentration.[11,12] The crack propagation rate of intergranular stress corrosion cracking (IGSCC) of stainless

*Corresponding author, Tel. +81-22-217-7911, Fax. +81-22-217-7900, E-mail: shunsuke.uchida@qse.tohoku.ac.jp

steel was moderated by the decreased ECP in the H_2O_2 environment as well as in the O_2 environment. However, when the concentration of H_2O_2 was lower than that of O_2 but the ECP remained the same, it was observed that the crack propagation rate in the H_2O_2 environment tended to be lower than that in the O_2 environment.[13]

Results of X-ray diffraction measurements of oxide films on stainless steel specimens exposed to H_2O_2 and O_2 environments showed that the difference in the ECP was mainly due to the chemical form of the oxide film on the stainless steel specimens.[14] Hematite (α-Fe_2O_3) was observed for the specimens exposed to H_2O_2 environment, while magnetite (Fe_3O_4) was the main oxide species when exposed to the O_2 environment.[14]

In order to confirm the difference in chemical form of the oxide films on the test specimens exposed to H_2O_2 and O_2 and to reveal the mechanism of oxide film formation, multi-analytical instrumentations were applied to examine the oxide film characteristics from a variety of viewpoints.

II. Experimental

1. Major Features of High Temperature, High Pressure Water Loop

The main features of the experimental apparatus are shown in **Fig. 1**.[11–14] The water, which was dearated in the make-up water tank and had its O_2 concentration controlled at the target level in the feed water tank, was fed to the autoclave through the regenerating heat exchanger and the main heater. The effluent water was polished by an ion exchange resin column to remove impurities and then fed back to the make-up water tank, where it was dearated to remove oxygen and prevent its accumulation from decomposition of H_2O_2.

The autoclave and hydrogen peroxide injection line and sampling line were lined with PTFE to prevent surface decomposition of H_2O_2. The work electrodes were installed in the autoclave to measure ECP while changing hydrogen peroxide concentration ([H_2O_2]) at the autoclave inlet.[11,13] In

order to quantify the corrosive environment, [H_2O_2] was measured in the sampling line located at the autoclave outlet, and ECP was also measured at several locations in the autoclave (bottom and top) (Fig. 1). Major parameters for the experimental loop are shown in **Table 1**. Observed ECPs for both specimens under the exposure conditions shown in Table 1 were the same, 0 mV-SHE.

2. Test Specimens

Test specimens exposed to the H_2O_2 environment (diameter: 20 mm, height: 20 mm, thickness: 1 mm) were cut from a cylinder-shaped upper SUS electrode for ECP measurement (**Fig. 2**(a)), while those exposed to the O_2 environment (width: 10 mm, height: 20 mm, thickness: 1 mm) were flat sheets, which were originally placed just above the upper SUS electrode in the loop for the purpose of surface characterization of the oxide film (Fig. 2(b)). The test specimens exposed to H_2O_2 were cut into four pieces to allow examination of their inner surface (Fig. 2(c)). As any differences in test specimen shape might cause some undesirable effects on precise

Table 1 Major parameters for the experimental loop

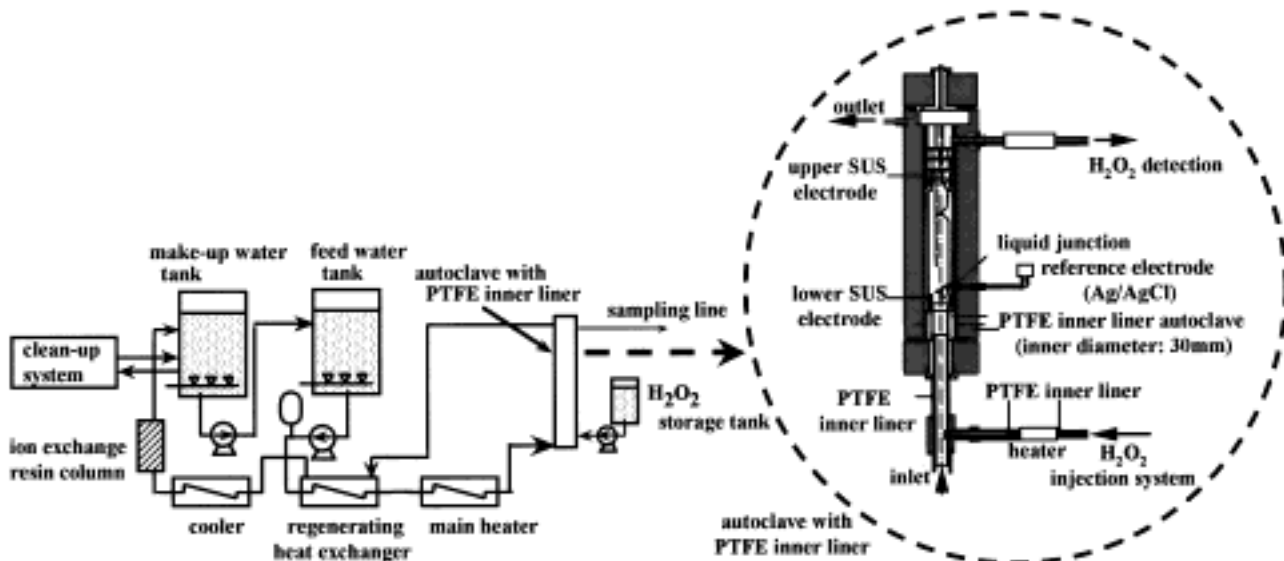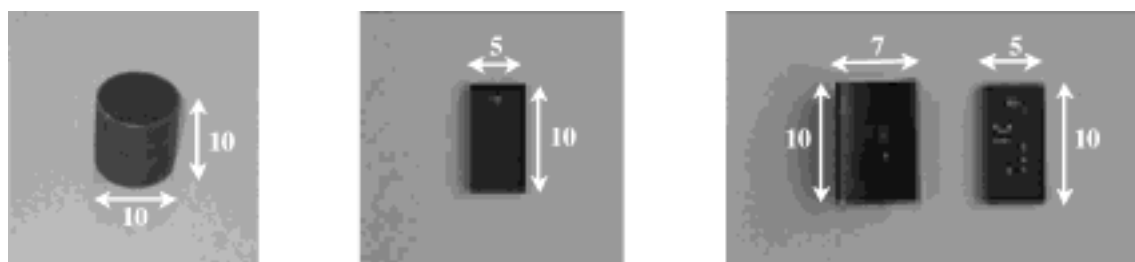| Item	Parameter	Parameter range
Autoclave	Temperature	561 K
	Pressure	6.9 MPa
	Flow rate	1–5 ml·s^{-1}
	Flow velocity	1–2 cm·s^{-1}
	Conductivity	<0.2 μS/cm
	[O_2]	0–8,000 ppb
	[H_2O_2]	0–1,000 ppb
Feed water tank	Temperature	280–300 K
	Pressure	0.1 MPa
	Conductivity	<0.2 μS/cm
	[O_2]	0–8,000 ppb
	[H_2O_2]	0 ppb

Fig. 1 Schematic diagram of high temperature, high pressure loop

(a) Test specimen exposed to H_2O_2 (b) Test specimen exposed to O_2 (c) Test specimen for SIMS   (Unit: mm)

Fig. 2 Outer views of test specimens

surface characterization, the authors wanted to understand the basic differences in oxide films exposed to H_2O_2 and O_2 environments before determining future approaches for the characterization. Both types of test specimens are made of sensitized type 304 stainless steel, which had the chemical composition shown in **Table 2**. Exposure conditions are shown in **Table 3**.

3. Multilateral Surface Analyses

Instruments for multilateral surface analyses to examine the oxide film characters are listed in **Table 4**. Chemical forms of the oxide films were observed by X-ray diffraction (XRD)[14] and laser Raman spectroscopy (LRS).[14] Furthermore, elemental composition and distribution through the depth of the films were measured by Rutherford back scattering (RBS)[15] and secondary ion mass spectroscopy (SIMS).[16] X-ray photoelectron spectroscopy (XPS)[17, 18] was applied to obtain information on the nearest top surface of the oxide films. For RBS, 2.8 MeV of He^{2+} ions were injected onto the surface of the specimen and the energy of the back scattered ions was analyzed to determine oxygen concentration along the oxide depth. For SIMS, 3 keV of Cs^+ ions were injected onto the surface of the specimen to sputter oxide in a very small spot and the secondary ions from the sputtered area were analyzed by mass spectroscopy. For XPS, monochromatic X-rays (Al-Kα: energy: 1,486.6 eV, energy width: 0.85 eV) were injected into the surface layers of the specimen, which was cleaned by exposing it to an Ar^+ ion beam to remove surface contamination, and then photoelectrons emitted from the oxide were measured.

III. Analytical Results

1. X-ray Diffraction (XRD) and Laser Raman Spectroscopy (LRS)

Surface characterization by XRD and LRS of the specimen exposed to almost the same environmental conditions was carried out previous to this study.[14] A comparison between XRD patterns for specimens exposed to H_2O_2 and O_2

Table 2 Chemical composition (mass%) of stainless steel used for the specimen

C	Si	Mn	P	S	Ni	Cr	Fe
0.06	0.42	0.83	0.028	0.005	8.41	18.31	Bal.

environments is shown in **Fig. 3**.[14] Clear peaks corresponding to hematite (α-Fe_2O_3) were observed for the specimen exposed to H_2O_2 while they were indistinct for O_2 exposure. At the same time, the peaks for the typical spinel of magnetite (Fe_3O_4) were observed clearly for the specimens exposed to O_2 but not for H_2O_2 exposure. Laser Raman spectroscopy was also applied to examine the surface properties of each specimen.[14] As a result of these analyses, it was revealed that hematite (α-Fe_2O_3) was the main oxide for the specimens exposed to H_2O_2 while magnetite (Fe_3O_4) was the main oxide when exposed to O_2.

2. Rutherford Back Scattering (RBS)

The RBS spectrum for each specimen type is shown in **Fig. 4**. The oxygen peak overlapped with the metallic atom peak in both cases. Change in energy of back scattered He^{2+} ions from the oxygen atoms is the smaller than that from each of iron, nickel and chromium atoms, while that from each metallic atom is very similar due to less difference in their mass numbers. The calculated spectrum for pure iron is plotted for comparison to a measured spectrum for each specimen. The observed drop in the metallic atom signal for the
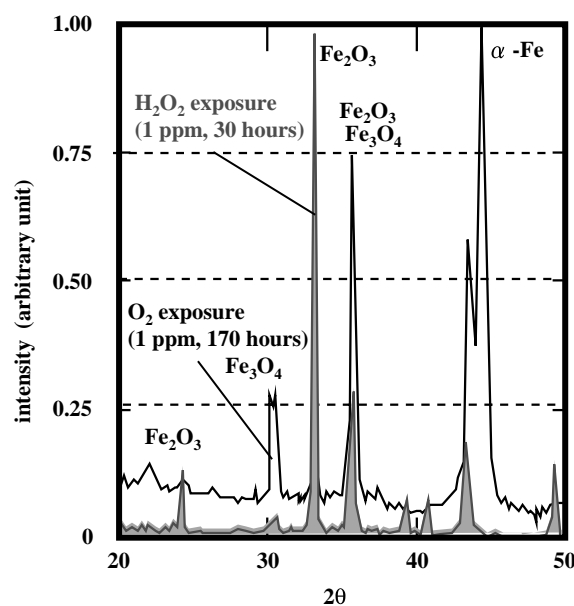

Fig. 3 Comparison between X-ray diffraction patterns for test specimens exposed to H_2O_2 and O_2 environments

Table 3 Exposure conditions

Specimen	Shape (size)	Material	Exposure (concentration)	Temperature (K)	Exposure time (h)
A	Cylinder (outer diameter: 10 mm)	Sensitized type 304 stainless steel	H_2O_2 (0.1–1 ppm)	558	200
B	Flat sheet ($10 \times 5 \times 1$ mm^3)	Sensitized type 304 stainless steel	O_2 (8 ppm)	558	200

Table 4 Instruments for multilateral surface analyses

Instruments	Incident beam	Beam size	Incident condition	Detected particles	Obtained information	Location of instruments
X-ray diffraction (XRD)	X-rays		Energy: 50 keV	Diffracted X-rays	Chemical form of oxide (average through film)	[1]
Laser Raman spectroscopy (LRS)	Visible rays		Wavelength: 632.8 nm	Scattered laser	Chemical form of oxide (thin layers of surface)	[1]
Rutherford back scattering spectroscopy (RBS)	He^{2+}	1 mmϕ	Energy: 2.8 MeV	Back scattered He^{2+}	Isotope distribution (through depth)	[2]
Secondary ion mass spectroscopy (SIMS)	Cs$^+$	$500 \times 500 \, \mu$m^2	Energy: 3 keV	Cs cluster	Isotope distribution (through depth)	[3]
X-ray photoelectron spectroscopy (XPS)	X-rays	4×4 mm^2	Energy: 1.486 keV	Photoelectrons	Chemical bonding (through depth)	[3]

[1] Power & Industrial Systems R&D Laboratory, Hitachi, Ltd
[2] Institute for Materials Research, Tohoku University
[3] Institute of Multidisciplinary Research, Tohoku University.
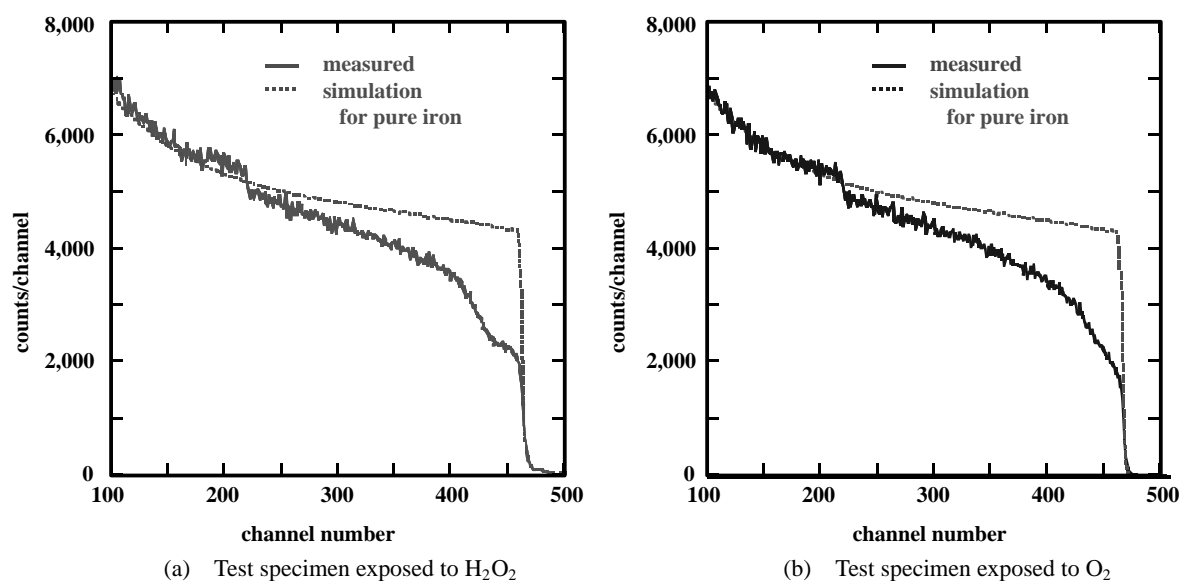

(a) Test specimen exposed to H_2O_2

(b) Test specimen exposed to O_2

Fig. 4 Rutherford backscattering spectra of He^{2+} for test specimens exposed to H_2O_2 and O_2 environments

measured spectrum is caused by the presence of oxygen in the oxide film. Comparing spectra for the specimens exposed to H_2O_2 (Fig. 4(a)) and O_2 (Fig. 4(b)) for channels 420–460, corresponding to the surface region showed small changes in the spectra worthy of attention. The much sharper drop observed only in the spectrum for the specimen exposed to H_2O_2 might be caused by a higher oxygen ratio in the oxide film.

By analyzing RBS spectral data, the depth profiles of the oxygen to iron ratio (O/Fe) were obtained and are shown in **Fig. 5**. To a depth of 0.1 μm, the specimen exposed to O_2 had a higher O/Fe ratio than that exposed to H_2O_2, while from 0.1 to 0.3 μm the specimen exposed to H_2O_2 had a much higher
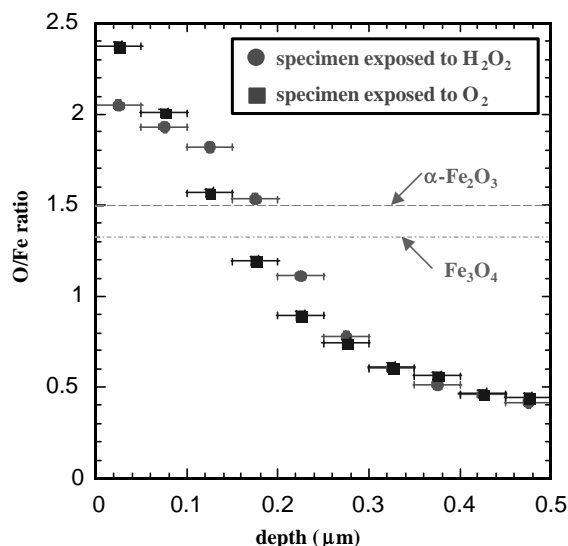
Fig. 5 Depth profiles of O/Fe in the test specimens measured by RBS

O/Fe ratio.

The O/Fe ratios in the depth region of less than $0.1\,\mu m$ were in excess of 1.5, the ratio of Fe_2O_3, and 1.33, that of Fe_3O_4, and were caused by crystal water contained in the oxide film or metal hydroxide, $Fe(OH)_2$ or $Fe(OH)_3$.

3. Secondary Ion Mass Spectroscopy (SIMS)

The test specimens were sputtered by $3\,keV$ of Cs^+ ions, which provided high resolution mass spectroscopy not only for metallic ions, but also oxygen and hydrogen ions. The oxygen/iron (O/Fe) and hydrogen/iron (H/Fe) ratios obtained from the SIMS spectrum for each specimen are shown in **Fig. 6**. In the case of SIMS, measured ion currents were affected not only by elemental composition in the oxide film but also their chemical forms, which caused the difference in sputtering yield and ionizing efficiency of the oxide.

Oxide layers with a constant O/Fe ratio were observed at the surfaces of the specimens (Fig. 6(a)). The O/Fe ratio drastically decreased as the depth increased. The thickness of oxide film on the stainless steel exposed to H_2O_2 was about $0.3\,\mu m$, while that to O_2 was about $0.2\,\mu m$.

A large difference was observed in the H/Fe ratios between specimens exposed to H_2O_2 and O_2. The H/Fe ratio of specimen A (Table 3) exposed to H_2O_2 was high and decreased steeply with depth. The H/Fe ratio at the very surface of the oxide film on the specimen exposed to H_2O_2 was much higher than that at the surface of the specimen B exposed to O_2 (Fig. 6(b)). The absolute ratio could not be discussed from the SIMS data. But the difference in the surface hydrogen concentrations at the surfaces provided important information on the oxidation mechanism for both corrosive circumstances. This enriched hydrogen content might come from OH radicals, which would be generated from H_2O_2 decomposition at the oxide surface.

Figure 7 shows Cr/Fe and Ni/Fe ratios. The specimen exposed to H_2O_2 showed Cr depression in the oxide film, while the specimen exposed to O_2 had Cr enrichment in the oxide

(Fig. 7(a)). No big difference in the Ni/Fe ratio was observed throughout the oxide film (Fig. 7(b)).

4. X-ray Photoelectron Spectroscopy (XPS)

Chemical bonding of each elemental component can be determined by the shift in binding energy of inner shell electrons due to their interaction with surrounding elements. Oxygen for hydroxide (OH^-) and that for oxide (O_2^-) can be identified by the $1–1.5\,eV$ of energy shift in the 1s electrons of the oxygen. The energy shift of metallic elements around oxygen was measured to analyze the difference in binding energy of metallic elements and oxygen in specimens exposed to H_2O_2 and O_2. Shifts in binding energy of O1s electrons measured by sputtering oxide films with Cs^+ ions are shown in **Fig. 8**.

The theoretical binding energy of O1s electrons is $531.0\,eV$. For specimen B exposed to O_2, the binding energy did not change with sputtering. The binding energy decreased to about $530.0\,eV$, which was caused by binding of oxygen atoms with metallic atoms as the oxides, Fe_3O_4 and α-Fe_2O_3. For specimen A exposed to H_2O_2, the binding energy without sputtering increased to about $531.5\,eV$, due to binding of oxygen atoms with hydrogen atoms as $Fe(OH)_n$. But the increasing energy shift was observed only at the very surface. After sputtering, the binding energy decreased to $530.0\,eV$. The effect of hydrogen was observed in several atomic layers. The effect of water on the test specimen was avoided for the XPS measurements by carefully controlling the vacuum.

IV. Discussion

1. Characterization of Oxide Films

As a result of X-ray diffraction measurements of oxide films on the stainless steel specimens exposed to H_2O_2 and O_2, hematite (α-Fe_2O_3) was observed for the specimens exposed to H_2O_2, while magnetite (Fe_3O_4) was the main oxide when exposed to O_2. Higher O/metal ratios were observed at the very surface of the oxide film by RBS. But it was difficult to discriminate between crystal water in the oxide and metal hydroxide by RBS analysis.

High hydrogen concentration at the oxide surface of the specimens exposed to H_2O_2 provides important information to understand the oxidation process. Hydrogen peroxide, which is rather stable in elevated temperature water, is easily decomposed at the oxide film surface. Hydrogen peroxide decomposes into two OH radicals, which are very short lived. At the oxide surface, a well-developed magnetite film can pick up some number of OH radicals to form a complex oxide containing hydrogen which is then dehydrated to give a higher order oxide (hematite).

Hydrogen presence was confirmed by the H/Fe ratio measurements. Direct measurement of OH might give much important information on the mechanism of hydrogen pick-up of the oxide film and chemical form change. Precise measurement of the oxide surface with X-ray photoelectron spectroscopy (XPS) might provide OH concentration in the film. To obtain clearer results from the XPS analysis, test specimens with a smoother and flatter surface should be prepared. Another topic to investigate is the surface character of the oxide film from which the oxidation mechanism of stainless
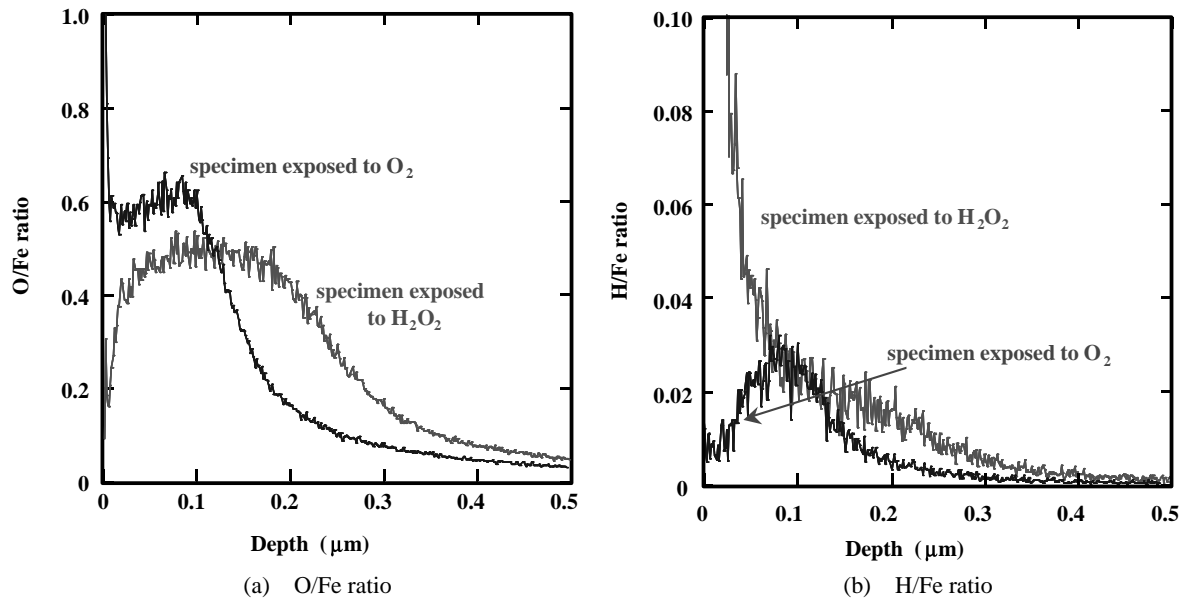
(a)   O/Fe ratio

(b)   H/Fe ratio

Fig. 6   Depth profiles of oxygen and hydrogen in test specimens measured by SIMS
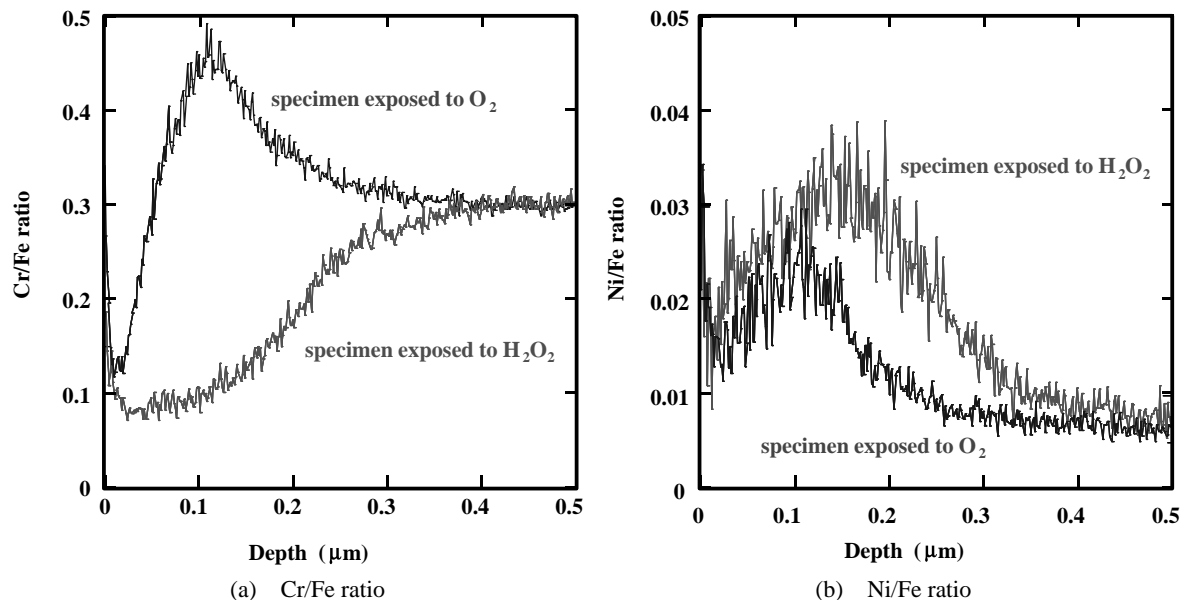

(a)   Cr/Fe ratio

(b)   Ni/Fe ratio

Fig. 7   Depth profiles of Cr and Ni in test specimens measured by SIMS

steel in the presence of H_2O_2 can be identified.

2. Effects of Oxide Character on Electrochemical Corrosion Potential (ECP)

The difference in ECP of stainless steel exposed to H_2O_2 and O_2 is caused by the difference in chemical form of oxide films, which consist mainly of hematite (α-Fe_2O_3) for H_2O_2 exposure and magnetite (Fe_3O_4) for O_2 exposure.

The difference in electric resistance of oxides causes the different in anodic polarization properties. In a previous paper,[19] the different anodic polarization curves were proposed to evaluate the experimentally obtained ECP data[8] for the specimens under O_2 and H_2O_2 environments. The authors tried to explain the difference in the anodic polarization

curves by electric resistance of the oxide films.

An Evans diagram to determine ECP is shown in **Fig. 9**. The ECP is defined as electric potential at the intersection point of the cathodic curve and the anodic curve. The anodic polarization curve of Hishida *et al.*[20] is also given in the figure, corresponding to the specimen under O_2 environment. When highly resistant oxide layers cover the specimen, the difference in potentials between the base metal and the surface of the oxide is caused by the anodic current and the electric resistance of the oxide layers. The anodic curve of the specimen under H_2O_2 environment can be determined by electric resistance of α-Fe_2O_3 (hematite) layers at the surface,
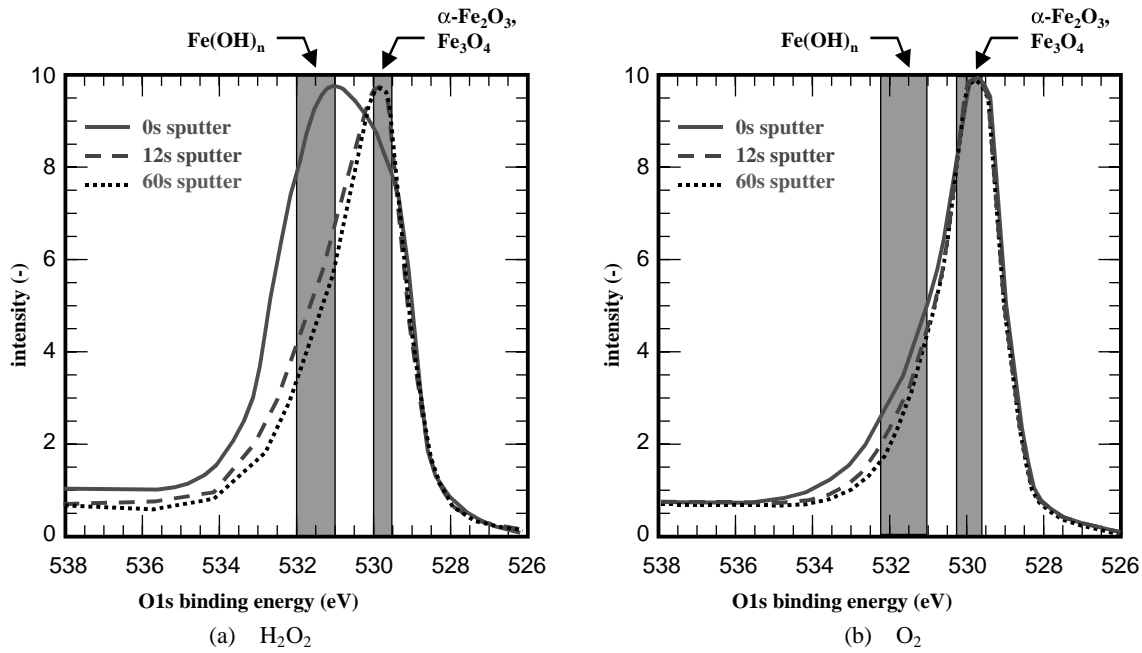
Fig. 8 Chemical binding states obtained from XPS spectra
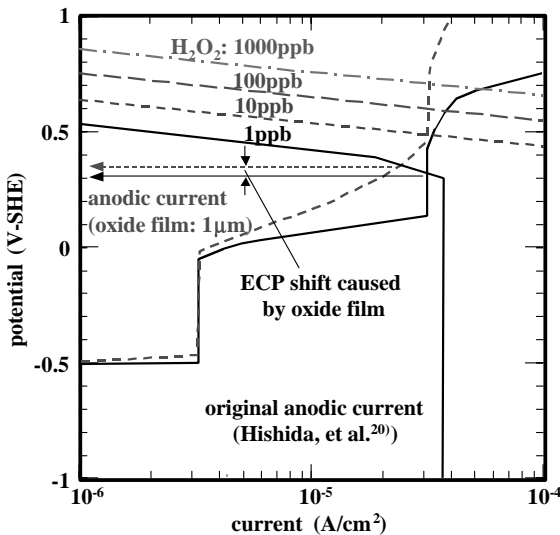

Fig. 9 Evans diagram to determine electrochemical corrosion potential (Effects of oxide film on anodic current)

which is as follows:

$$I_a = I(V) \qquad \text{without surface electric resistance} \qquad (1)$$

$$I_a = I(V - I_a R_f)$$

$$\text{with surface electric resistance, } R_f \qquad (2)$$

$$I_a = I^*(V, R_f). \qquad (3)$$

Specific resistance of magnetite (Fe_3O_4: semiconductor) is about 10^{-4} $\Omega \cdot$m, while that of hematite (Fe_2O_3: insulator) is estimated as 3×10^6 $\Omega \cdot$m (about 1/100 of that of Al_2O_3).[21] These data are obtained by extrapolating from those measured at room temperature.

Calculated anodic polarization curves for 10^4 Ω/cm^2 of R_f

(oxide film thickness: 0.3 μm) are shown in Fig. 9. As a result of decreasing anodic current, ECP of the specimen with an oxide film increased, while corrosion current decreased.

3. Further Subjects for Oxide Characterization

A drop in chromium concentration in the oxide film on the specimens exposed to H_2O_2 was confirmed, which resulted in less corrosion resistance to enhance general corrosion of stainless steel in coolant containing H_2O_2. Opposite effects of H_2O_2 on corrosion of stainless steel should be discussed for depression of corrosion resistance due to loss of chromium in the oxide layers on the specimen exposed to H_2O_2 and decrease of corrosion current due to ECP increase by increasing electric resistance of hematite in the oxide film.

Electric resistance of oxide film should be determined for both H_2O_2 and O_2 exposed specimens to estimate the shift in anodic polarization curves due to oxide layers. At the same time, it is recommended that several anodic polarization curves should be prepared for different surface conditions to calculate ECP based on the Evans diagram.

V. Conclusions

The conclusions are summarized as follows.
(1) A highly ordered oxide film was confirmed by X-ray diffraction (XRD) and Rutherford back scattering spectroscopy (RBS) measurements.
(2) Depressed chromium concentration was observed at the oxide film on the specimens exposed to H_2O_2, which might cause formation of an unstable oxide film and then enhanced general corrosion.
(3) Enriched hydrogen concentration at the oxide surface of the specimens exposed to H_2O_2 might be caused by pick-up of OH radicals which came from hydrogen peroxide decomposition at the oxide surface.

(4) One possible mechanism for forming highly ordered oxide at the oxide film surface of the specimens exposed to H_2O_2 was that OH radicals picked up in the oxide film formed a complex oxide containing hydrogen and then these was dehydrated to get a higher order oxide (hematite).

It was confirmed that multilateral analysis can prepare valuable information to understand the difference in oxide films of specimens exposed to H_2O_2 and O_2 from which the mechanism of oxidation of stainless steel under H_2O_2 exposure can be proposed. Much precise measurements should be carried out by preparing well-arranged test specimens in the high temperature, high pressure experimental loop.

Nomenclature and Abbreviation

$I(V)$, $I^*(V, R_f)$: Function of V or V and R_f
I_a: Anodic current (A/m^2)
V: Potential (V-SHE)
R_f: Surface electric resistance (Ω/m^2)

BWR: Boiling water reactor
ECP: Electrochemical corrosion potential
HWC: Hydrogen water chemistry
IGSCC: Intergranular stress corrosion cracking
LRS: Laser Raman spectroscopy
PTFE: Polytetrafluoroethylene
RBS: Rutherford back scattering spectroscopy
SIMS: Secondary ion mass spectroscopy
XPS: X-ray photo-electron spectroscopy
XRD: X-ray diffraction

Acknowledgment

References

1) R. L. Cowan, "The mitigation of IGSCC of BWR internals with hydrogen water chemistry," *Proc. Int. Conf. Water Chemistry of Nuclear Reactor Systems, Water Chemistry 7*, British Nuclear Energy Society, 196 (1996).

2) H. Takiguchi, M. Sekiguchi, A. Abe, *et al.*, *J. Nucl. Sci. Technol.*, **36**, 179 (1999).

3) Y. Wada, S. Uchida, M. Nakamura, *et al.*, *J. Nucl. Sci. Technol.*, **36**, 169 (1999).

4) S. Uchida, E. Ibe, K. Nakata, *et al.*, *Nucl. Technol.*, **110**, 250 (1995).

5) R. J. Row, M. E. Indig, C. C. Lin, *et al.*, "Suppression of radiolytic oxygen produced in a BWR by feedwater hydrogen addition," *Proc. Int. Conf. Water Chemistry of Nuclear Reactor Systems, Water Chemistry 3*, British Nuclear Energy Society, 23 (1984).

6) R. L. Cowan, M. E. Indig, J. N. Kass, *et al.*, "Experience with hydrogen water chemistry in boiling water reactors," *Proc. Int. Conf. Water Chemistry of Nuclear Reactor Systems, Water Chemistry 4*, British Nuclear Energy Society, 29 (1986).

7) F. P. Ford, D. F. Taylor, P. L. Andresen, *et al.*, EPRI NP-5064M Project 2006-6 Final Report, (1987).

8) Y. J. Kim, L. W. Niedrach, C. C. Lin, *et al.*, "Development of ECP models for BWR application," *Proc. 7th Int. Symp. Environmental Degradation of Materials in Nuclear Power Systems—Water Reactors*, Breckenridge, CO., National Association of Corrosion Engineers, 699 (1995).

9) C. C. Lin, F. R. Smith, N. Ichikawa, *et al.*, *Int. J. Chem. Kinet.*, **23**, 971 (1991).

10) D. Hiroishi, "Homogeneous and heterogeneous decomposition of hydrogen peroxide in high temperature water," *Proc. Int. Conf. Water Chemistry of Nuclear Reactor Systems, Water Chemistry 5*, British Nuclear Energy Society, 311 (1989).

11) S. Uchida, N. Shigenaka, M. Tachibana, *et al.*, *J. Nucl. Sci. Technol.*, **35**, 301 (1998).

12) S. Uchida, M. Tachibana, A. Watanabe, *et al.*, *J. Nucl. Sci. Technol.*, **37**, 257 (2000).

13) Y. Wada, A. Watanabe, M. Tachibana, *et al.*, *J. Nucl. Sci. Technol.*, **37**, 901 (2000).

14) Y. Wada, A. Watanabe, M. Tachibana, *et al.*, *J. Nucl. Sci. Technol.*, **38**, 183 (2001).

15) W. K. Chu, J. W. Mayer, M. A. Nicolet, *Backscattering Spectrometry*, Academic Press, New York, (1978).

16) J. C. Vickerman, A. Brown, N. M. Reed, *Secondary Ion Mass Spectrometry: Principles and Applications* (International Series of Monographs on Chemistry: Vol. 17), Clarendon Press: New York, (1989).

17) D. Briggs, M. P. S. Chichester, *Practical Surface Analysis: by Auger and X-ray Photo-Electron Spectroscopy*, Wiley, New York, (1983).

18) J. F. Moulder, W. F. Stickle, P. E. Sobol, K. D. Bombern, *Handbook of X-ray Photoelectron Spectroscopy*, Perkin-Elmer Corp., Physical Electronics Division: Eden Prarie, MN, (1992).

19) Y. Wada, A. Watanabe, M. Tachibana, *et al.*, "The electrochemical corrosion potential and stress corrosion cracking of 304 stainless steel under low hydrogen peroxide concentrations," *Proc. 9th Int. Symp. Environmental Degradation of Materials in Nuclear Power Systems—Water Reactors*, Newport Beach, CA., National Association of Corrosion Engineers, 339 (1999).

20) M. Hishida, J. Takabayashi, T. Kawakubo, *et al.*, *Corrosion NACE*, **41**, 570 (1985).

21) Nihon-kagakukai, *Kagaku Binran*, II-493, Maruzen, (2001), [in Japanese].